Current Eye Research, 32:851–861, 2007

ISSN: 0271-3683 print / 1460-2202 online
DOI: 10.1080/02713680701585872

informa
healthcare

Assessment of Rat and Mouse RGC Apoptosis Imaging *in Vivo* with Different Scanning Laser Ophthalmoscopes

Annelie Maass
Glaucoma & Retinal Neurodegeneration Research Group, Institute of Ophthalmology, University College London, London, United Kingdom

Peter Lundh von Leithner and Vy Luong
Visual Science, Institute of Ophthalmology, University College London, London, United Kingdom

Li Guo
Glaucoma & Retinal Neurodegeneration Research Group, Institute of Ophthalmology, University College London, London, United Kingdom

Thomas E. Salt and Frederick W. Fitzke
Visual Science, Institute of Ophthalmology, University College London, London, United Kingdom

M. Francesca Cordeiro
Glaucoma & Retinal Neurodegeneration Research Group, Institute of Ophthalmology, University College London, London, United Kingdom

ABSTRACT *Purpose*: We have recently described a novel way of imaging apoptosing retinal ganglion cells *in vivo* in the rat. This study investigated if this technique could be used in the mouse, and whether the Heidelberg Retina Angiograph II (HRAII) was appropriate. *Methods*: Retinal ganglion cell (RGC) death was induced by intravitreal injections in rat and mouse eyes using staurosporine. Fluorescent-labeled apoptosing cells were detected by imaging with both the HRAII and a prototype Zeiss confocal scanning laser ophthalmoscope (cSLO). Averaged *in vivo* images were analyzed and results compared with histologic analysis. *Results*: Fluorescent points (FPs) used as a measure of RGC apoptosis *in vivo* were detected in the mouse eye but only with the HRAII and not the Zeiss cSLO. The HRAII was able to detect 62% more FPs in rat than the Zeiss cSLO. Both cSLOs showed peak FP counts at the 5- to 10-μm range in rat and mouse. Maximal FP counts were detected in the superior and superior temporal regions in the rat, with no obvious pattern of distribution in the mouse. The HRAII was found to have more FP correspondence with histologically identified apoptosing RGCs. *Conclusions*: To our knowledge, this is the first demonstration of visualized apoptosing RGC *in vivo* in a mouse. The improved image quality achieved with the HRAII compared with the Zeiss cSLO was validated by histology. This together with its enhanced maneuverability and the fact that it is already commercially available make the HRAII a potential tool for the early detection and diagnosis of glaucomatous disease in patients.

KEYWORDS apoptosis; *in vivo* imaging; mouse model; retinal ganglion cell

INTRODUCTION

We have recently described a new way of imaging single apoptosing retinal ganglion cells (RGCs) *in vivo* using confocal laser scanning ophthalmoscopy (cSLO).[1] This technique enables the visualization of single nerve cell apoptosis and is an important advance for longitudinal studies of disease processes, because until now it has only been possible to assess RGC apoptosis histologically.

Apoptosis is a type of cell death where the cell is "programmed" to "commit suicide" when it has been sufficiently damaged or is no longer needed.

Received 26 January 2007
Accepted 16 July 2007

Correspondence: M. Francesca Cordeiro, Glaucoma & Retinal Neurodegeneration Research Group, Institute of Ophthalmology, University College London, 11-43 Bath Street, EC1V 9EL London, UK. E-mail: M.Cordeiro@ucl.ac.uk

It occurs in physiological and pathological conditions, including neurodegenerative such as Alzheimer's, Huntington's, Parkinson's and stroke.[2–4] An early feature in the apoptotic process, before DNA fragmentation and nuclear condensation occurs, is the externalization of phosphatidylserine (PS).[5,6] PS is a phospholipid that, in a healthy cell, is normally situated in the inner leaflet of the plasma membrane. Fluorescent-labeled Annexin V has a strong affinity to bind to externalized PS and is therefore a useful tool to detect cells undergoing apoptosis.[7]

The first visualization of basic cellular physiologic and pathologic processes within the living organism was made by Wilhem Conrad Röntgen in 1895.[8] Many methods have since followed, including magnetic resonance imaging (MRI) and positron emission tomography (PET)[9–11] Although the pathologic substrate of disease can be studied at the tissue level with these techniques, the assessment of biological processes within single cells of an intact living organism has not been previously possible.[12]

Confocal scanning laser ophthalmoscopy (cSLO) was introduced in the late 1980s [13] and is widely used both clinically and in research[14,15] especially in the diagnosis and monitoring of glaucoma disease.[16–18] Currently, the most popular SLO instrument is the Heidelberg Retinal Tomograph (HRT). The HRT produces topographical images of the optic nerve head (ONH), by the processing of 32 transverse sections, with a 200- to 300-μm depth resolution[19–21] and can be used for the monitoring of ONH changes. However, it cannot be used with our novel technique of imaging apoptosing retinal cells as it has no blue laser.[1]

An adaptation of the HRT is the Heidelberg Retinal Angiograph (HRA), which, because of its ability to detect fluorescence, is utilized in the technique of fundus autofluorescence (FAF)[22] and fluorescein angiography clinically.[23–25] FAF imaging has been developed and improved over the past decade and became a very important diagnostic tool in a variety of retinal diseases.[26,27] It enables the visualization of the retinal pigment layer by identifying intrinsic (lipofuscin) autofluorescent signals,[24,26–28] revealing characteristic patterns in different hereditary disorders (e.g., Stargardts).[29] Our previous publications looking at our novel technique of imaging apoptotic RGCs were based solely on the histologic counts as we needed to establish colocalization to the retinal ganglion cell layer.[1,30] However, all our data suggest the process of apoptosis induced by staurosporine (SSP) is localized to RGCs and therefore any *in vivo* apoptotic signal, we believe, should reflect RGC damage. In this study, for the first time we are using the *in vivo* apoptotic signal as a measure of RGC apoptosis.

Over the past century, the mouse has developed into an extremely important mammalian model system for genetic and basic cell biological research. Scientists from a wide range of biomedical fields have gravitated to the mouse because of its genetic and physiologic similarities to humans, as well as the ease with which its genome can be manipulated and analyzed. A large genetic reservoir of potential models of human disease has been generated through the identification of more than 1000 spontaneous, radiation-induced, or chemically induced mutant loci.[31] Numerous transgenic mice are available with genetic changes that are very important for understanding retinal and visual function.[32–34] In addition, a number of recent technological advances have dramatically increased our ability to create mouse models of human disease.

The aims of this study were firstly to assess if our novel technique of identifying fluorescent-labeled apoptotic retinal ganglion cells *in vivo* with Annexin V[1] was possible to apply to the mouse eye; secondly, to determine if the commercially available Heidelberg Retina Angiograph II (HRAII, Heidelberg, Germany) could be used with this method; and finally, to compare *in vivo* results with confocal histology.

MATERIALS AND METHODS

Animal Models

All animals were treated with procedures approved by the UK Home Office and in compliance with the ARVO Statement for the Use of Animals in Ophthalmic and Vision Research. For all studies, we employed our SSP-induced RGC apoptosis model.[1,30] Adult Dark Agouti rats, (n = 3) and asult C57 mice (n = 6) were anesthetized by intraperitoneal injection using a mixture of ketamine (37.5%), dormitor (25%), and sterile water (Pfizer Animal Health, Exton, PA, USA) at 0.2 ml/100 g. RGC death was induced by intravitreal injections with SSP 1.07 nmol in PBS; at the same time,

TABLE 1 Comparison of the technical properties of the HRAII and the prototype Zeiss cSLO

Characteristic	HRAII	Zeiss cSLO
Laser type	488 nm argon	488 nm argon
Barrier filter	500 nm	521 nm
Laser output	275 μm	320 μm
Detector type	Photodiode	Photomultiplier tube
Field of view	15°/20°/30°	20°/40°
Confocal aperture	400 μm	2 mm
Image dimensions	1536 × 1536 px/768 × 768 px	768 × 576 px
Nominal micrometers per pixel	1.15 (Rat)	3.07 (Rat)
	0.61 (Mouse)	1.61 (Mouse)
Exposure time per frame	0.125 s	0.04 s
Frame rate	8 frames/s	25 frames/s
Total exposure time for acquired sequence	32 s	10 s

px, pixels.

Annexin V labeled with Alexa fluor 488 (0.5 μg/μl) (ex = 493 nm, em = 517 nm) was given to label apoptotic cells so that a final total volume of 5 μl (rats) and 1 μl (mice) containing both agents was given to all eyes.[1,30] All agents were injected into the vitreous body under microscopic visualization with the aid of a 5-μl Hamilton syringe (Hamilton Company, Reno, NV, USA) with a 34-gauge/8-mm length Hamilton metal needle using a motorized syringe pump to allow slow and controlled delivery (UMP2; World Precision Instrument, Sarasota, FL, USA). The eye was punctured at approximately 1 mm posterior to the limbus at the most apical point, and the needle was held at a 45° angle throughout the injection. Caution was taken to avoid contact with the lens.

Identification of RGCs

For identification of normal RGCs, two adult C57 mice had RGCs retrogradely labeled by the application of 1,1′-dioctadecyl-3,3,3′,3′-tetramethylindocarbocyanine perchlorate (DiI; $DiIC_{18}$ (3)) (Molecular Probes, Eugene, OR, USA) to both superior colliculi by a method we have described.[1,30,35] Seven days after the DiI labeling, the mice underwent staurosporine (SSP) and Annexin V treatment. Hematoxylin-stained cross sections of histologic eyes were examined and scanned by confocal microscopy to confirm that Annexin V staining was at the RGC layer as we described before. We have previously shown that RGCs labeled with fluorescent-labeled Annexin are apoptotic by using double labeling with an anti-caspase 3 antibody.[1]

Comparison of the Technical Properties of Both SLOs (Zeiss cSLO/HRAII)

To allow accurate comparison between machines, set parameters were used to define instrumentations. Table 1 summarizes technical properties of each machine. Several differences are evident between both machines. Emitted fluorescent light is detected above 500 nm for the HRAII and above 521 nm for the Zeiss cSLO (long-pass cutoff filter). The laser output at the cornea surface is constant at 320 μW for the Zeiss cSLO and 275 μW for the HRAII. The older design of the Zeiss cSLO employs a broadband Hamamatsu photomultiplier tube (PMT), whereas the HRAII incorporates an Avalanche Photodiode detector (APD). The pivotal axes of the two machines are different—the radius of the HRAII is greater in horizontal and vertical directions, which enables a maximum field of view of 110° × 115° compared with the Zeiss cSLO with only 90° × 90°. This allowed us to obtain a maximum of 12–15 single images compared with a maximum of 9 with the Zeiss cSLO; however, for the purposes of this study, comparison was made of 9 single images per eye with both machines. Each single image obtained with the HRAII consists of 768 × 768 pixels (15° field of view) or 1536 × 1536 pixels (30° field of view), and images obtained with the Zeiss cSLO consist of 768 × 576 pixels (40° field of view). For calibration in order to measure retinal ganglion cell size, we used values of 59 μm at the retina for 1° of visual angle subtended at the rat eye,[36] which corresponds with 1.15 μm/pixel for the HRAII for both the 15° and 30° fields and

3.07 μm/pixel for the 40° field with the Zeiss. For the mouse eye, using values of 31 μm/degree[36] gives values of 0.61 μm/pixel for the HRAII and 1.61 μm/pixel for the Zeiss. The actual resolution limits would be determined by refractive error, aberrations, and other limiting factors due to the optics of the eye.

Imaging

A prototype Carl Zeiss cSLO SM30-4024 (CZ; Carl Zeiss AG, Oberkochen, Germany) and a Heidelberg Retinal Angiograph II (HRAII; Heidelberg Engineering GmbH, Heidelberg, Germany) were used in this comparative study. The Zeiss cSLO imager had been optimized for fluorescence detection in an earlier study.[27] The technical and optical characteristics of the HRA machine have been described previously.[22–25] Briefly, oscillating mirrors allow horizontal and vertical beam scanning, and the refractive error is corrected within the range of ±12 diopters. The system uses a 3-mm illumination beam aperture and the full aperture of the dilated pupil to collect the emitted fluorescence light. The confocal detection unit employs a small pinhole aperture (400 μm) allowing scattered light and light originating from structures outside the focal plane to be efficiently suppressed resulting in a high-contrast image compared with a nonconfocal image.

For imaging, all animals were held in a stereotaxic frame. To optimize visualization,[37] eyes were lubricated regularly and supplemental topical anesthesia was achieved with proxymetacaine. Pupils were dilated with one drop each of phenylephrine hydrochloride 2.5% and cyclopentolate hydrochloride 1.0%.

Retinal images were taken from 1 hr after SSP intravitreal injections, and imaging was performed of the same eyes using the prototype Zeiss cSLO and a HRAII in a randomized order. The laser output at the cornea surface was measured with an UDT radiometric meter (optometer model 370/radiometric detector head model 221; UDT Instruments, Baltimore, MD, USA) and a NOVA laser power monitor (Ophir, Laser Measurement Group, Ophir Optronics LTD, Jerusalem, Israel). Images were obtained using a 15° field of view mode (mice) or 30° field of view mode (rats) on the HRAII and a 40° field of view on the Zeiss cSLO, as previously established.[1,38]

During image acquisition, cSLOs were focused on the retinal nerve fiber layer, as identified in the reflectance mode.

Image Processing

The same method of image postprocessing was used for the Zeiss cSLO and the HRAII. All images were recorded as sequences of 250 frames to obtain a low-noise, high-contrast single image. By averaging all aligned 250 frames, the signal-to-noise-ratio (SNR) was drastically improved. Brightness and contrast values were manually adjusted using the same values for all single images to maintain comparability (Adobe Photoshop 7.0; Adobe Systems Inc., San Jose, CA, USA). The resulting single images (n = 90) were analyzed for fluorescent point (FP) counts. These point counts were used as a way of assessing RGC apoptosis.

Fluorescent Point Counts

To quantify the FP counts, we employed Metamorph software (Universal Imaging Corp., West Chester, PA, USA). Each single image (n = 90) was intensity thresholded for light objects until the FPs would appear as clearly accentuated objects on a black background. Using the "Integrated Morphometry Analysis" (IMA) function, we set the size filter (equivalent radius) to a fixed range of 2.5–15 μm. Automated counts were performed by using the "Measure" function, which allowed us to ascertain the total number of FPs in each image. Data was immediately recorded applying the "configure log and open log" function to a Microsoft Excel (Redmond, WA, USA) spreadsheet.

The FP distribution in relation to size and according to its respective retinal image location in rat and mouse was analyzed by calculating mean values per single *in vivo* averaged image (n = 90) with 95% confidence intervals. Multiple comparisons between both SLO techniques were performed using ANOVA. Comparison between both techniques with regard to the measurement of FP was done using a Bland/Altman plot where, as there is no established gold standard measure, FP counts were compared with the average calculated from both machines.[39]

Apoptotic FP density counts were calculated from manual FP counts in the corresponding measured retinal areas using image analysis software (Matrox Inspector 3.1; Matrox Electronic Systems Ltd, Quebec, Canada), to obtain average FP counts per mm^2 (FP density). Comparisons between *in vivo* apoptotic FP density and confocal histology apoptotic RGC density were performed using ANOVA, showing mean values with standard errors (SEM).

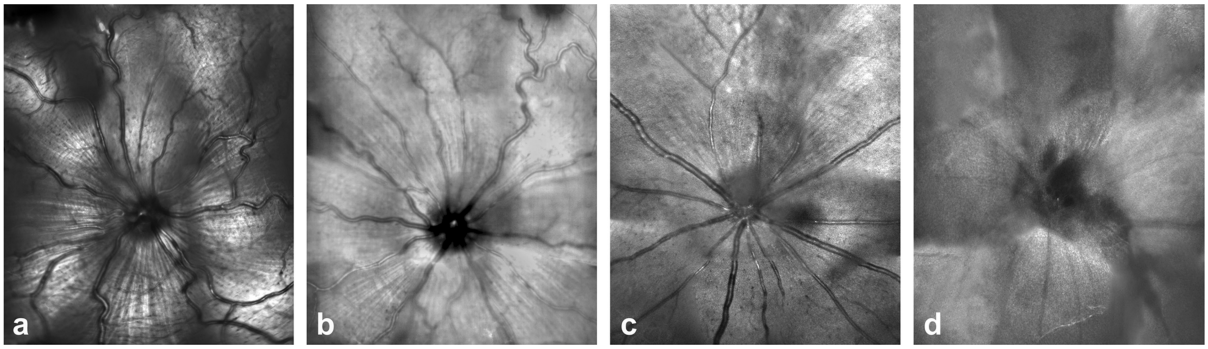

FIGURE 1 Retinal reflective images obtained *in vivo* in the rat with the (a) HRAII and the (b) Zeiss cSLO and in the mouse with the (c) HRAII and the (d) Zeiss cSLO.

Assessment of RGC Apoptosis Density Using Confocal Histology

The animals were sacrificed immediately after cSLO imaging. The eyes were enucleated and fixed in 4% fresh paraformaldehyde overnight. The retinas were dissected and whole flat retinas were mounted as we have described.[1,35] The flat retinas were examined with a confocal laser scanning microscope (CLSM 510 META; Zeiss) and processed with imaging software (CLSM 510 META; Carl Zeiss, Jena, Germany; Meditec, Inc., Oberkochen, Germany). Using ×16 magnification, we assessed 81 adjacent microscopic fields (each measuring 0.329 mm^2) for the rat and 65 adjacent microscopic fields (each measuring 0.329 mm^2) for the mouse, accounting for 40% of the whole retina. A retinal montage was then made for each whole retina.[1,35] The cell density of apoptotic RGCs (labeled with Annexin V) was then calculated using the same method described above for *in vivo* FP density.

RESULTS

Reflectance Images and Fluorescence Imaging (Rat versus Mouse)

A comparison between HRAII and Zeiss cSLO images is shown in Figure 1. Although both ophthalmoscopes show satisfactory results in the rat within the reflectance mode (Fig. 1a, b), this is not true with respect to the mouse–and in fact we were unable to obtain good quality reflective images in the mouse with the Zeiss cSLO (Fig. 1d) but did with the HRAII (Fig. 1c).

Figure 2 illustrates differences between images acquired by both machines using the blue Argon laser at 488 nm. There is an obvious difference in sensitivity between the HRAII (Fig. 2a) and the cSLO (Fig. 2b) in rat. As with the reflectance mode, we were unable to obtain a good quality mouse fluorescent retinal image with the Zeiss cSLO (Fig. 2d) compared with the HRAII (Fig. 2c).

Fluorescence Detection (Rat versus Mouse)

As the limitations of the Zeiss made it impossible to perform a detailed analysis of the mouse eye, we

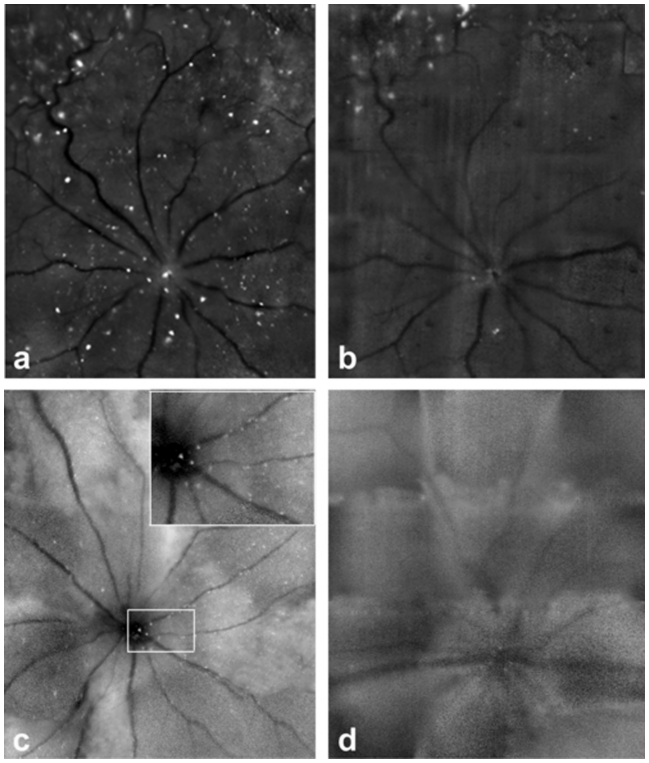

FIGURE 2 Retinal fluorescence images obtained *in vivo* with the (a, c) HRAII and the (b, d) Zeiss cSLO of the same retinae in (a, b) rat and (c, d) mouse. The numerous fluorescent points (FPs) are evident in the enlarged area outlined in (c) The increased resolution of the HRAII is clearly visible.

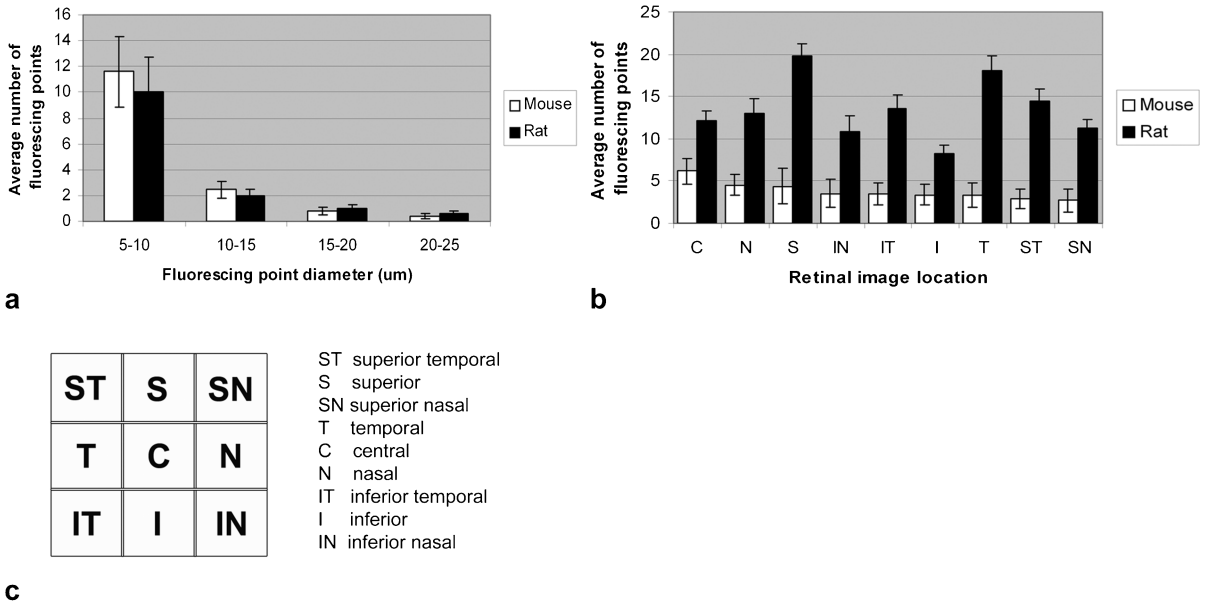

FIGURE 3 **Comparison of the FP size distribution between rat and mouse obtained by the HRAII. (a) Most fluorescent counts were obtained in the 5- to 10-μm size range in both rats and mice (a). (b) A comparison of the average number of FPs between rat and mouse according to its respective retinal image location is shown. (c) There is no pattern of distribution of FPs in relation to retinal image location, although the fluorescence is more evenly distributed in the mouse retina.**

compared the different fluorescent point profiles detected in the rat and mouse obtained by the HRAII.

Figure 3a shows a comparison of the fluorescent point distribution in relation to size between rat and mouse obtained by the HRAII. Both animals show a skewed distribution with maximal detection at 5–10 μm. At the smaller size intervals (5–10 μm and 10–15 μm), fluorescent point counts in the mouse show a higher number than in the rat. At the larger size intervals (15–20 μm and 20–25 μm), FP counts in the rat show a higher number than in the mouse; however, these differences are not statistically significant.

Figure 3b, c shows the mean number of fluorescent points per single frame according to its respective retinal image location. There seems to be no correlation between the pattern of fluorescent points according to its retinal image location in the rat compared with the mouse eye. The highest density of fluorescent points in the mouse was found to be around the optic nerve head in the central (C) area. In the rat, we discovered the highest density of fluorescent points in the superior (S), temporal (T), and superior temporal (ST) regions with a trend for more fluorescent points to be located superiorly compared with inferiorly.

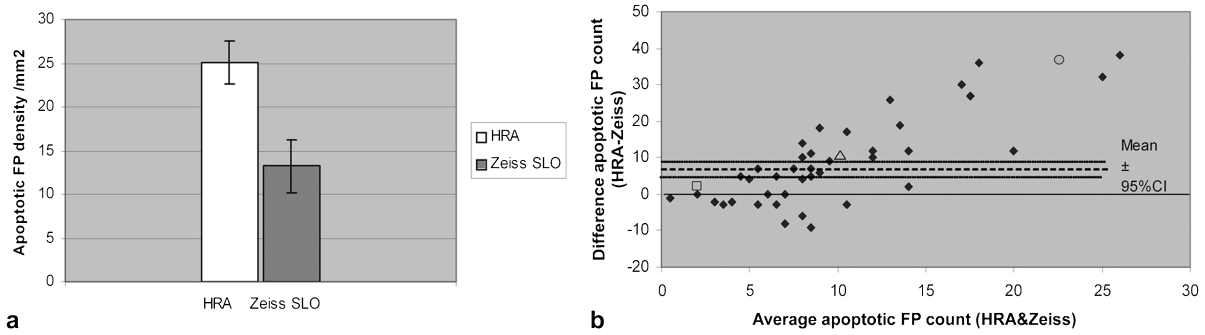

FIGURE 4 **Comparison of apoptotic FP density (HRA vs. Zeiss). (a) The average number of apoptotic FPs per mm^2 in rats was 25 for the HRAII and 13 for the Zeiss cSLO. This suggest that the HRAII picks up 1.9 times more fluorescence signal compared with the Zeiss cSLO. (b) The difference between HRAII and Zeiss FP counts plotted against the average combined HRAII and Zeiss count shows a positive trend suggesting the HRAII is more sensitive at detecting smaller point signals. The marked data points highlight typical points, detailed in the text for comparison.**

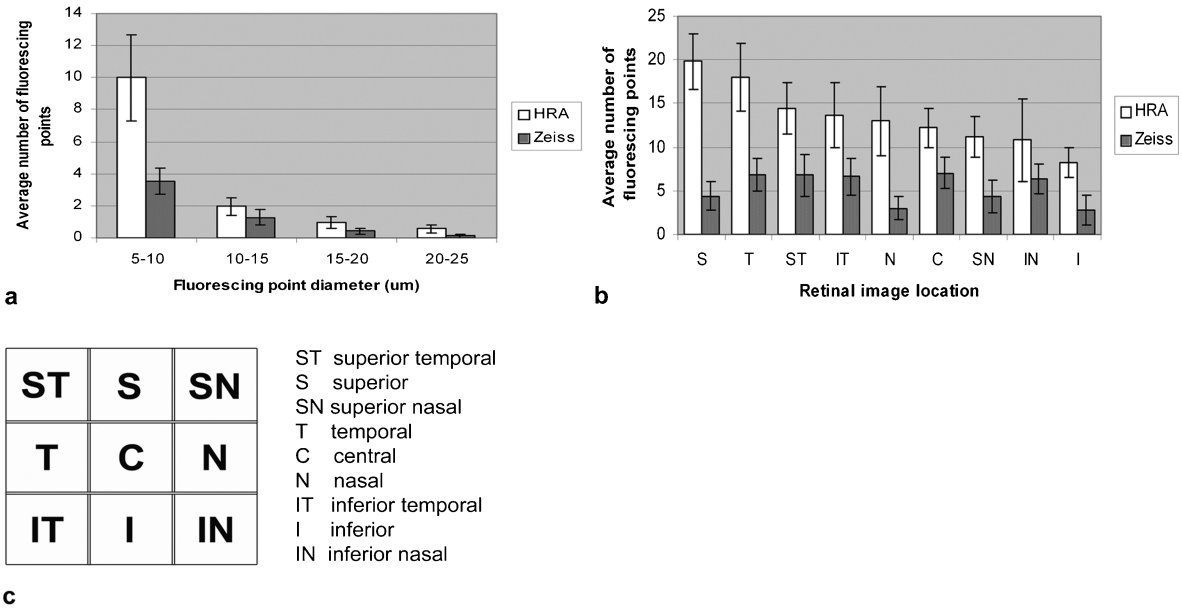

FIGURE 5 **FP distribution in relation to (a) their diameter size and (b, c) the retinal image location in the rat. On average, the Zeiss detects 60% less fluorescent signal compared with the HRAII. The majority of FPs were within the 5- to 10-μm size range and the count number gradually decreased with increasing point diameter (a). The average number of FPs per single frame according to its respective retinal image location is shown in (b) with the corresponding retinal image map (c).**

Comparison of the HRAII and Zeiss cSLO

Comparison of FP Density

The average number of FP counts per mm^2 in rats was 25 for the HRAII and 13 for the Zeiss cSLO (Fig. 4a). This suggests that the HRAII picks up 1.9 times more fluorescence signal compared with the Zeiss cSLO. The Bland/Altman plot of the FP shows a positive trend (Fig. 4b) suggesting the HRAII is more sensitive at detecting smaller point signals than the Zeiss cSLO. This is more clearly explained by looking at individual data points. The open square data point (Fig. 4b) shows a point with an average point count of 2 and a difference of only +2 between the SLOs, which corresponds in actual terms with the HRAII detecting 3 points and the Zeiss 1 point. Similarly, the open triangle data point with an average point count of 10 and a difference of +10 corresponds with 15 and 5 points on the HRAII and Zeiss, respectively. Finally, the difference in sensitivity between machines is clearly illustrated by the open circle data point in Figure 4b, where an average point count of 22.5 and a difference of +37 corresponds with the HRAII picking up 41 points compared with the Zeiss cSLO, which detected only 4.

Comparison of FB Distribution

We analyzed the FP size distribution in rat eyes (Fig. 5a). There is a decreasing trend between the number of FPs detected and their point size such that the

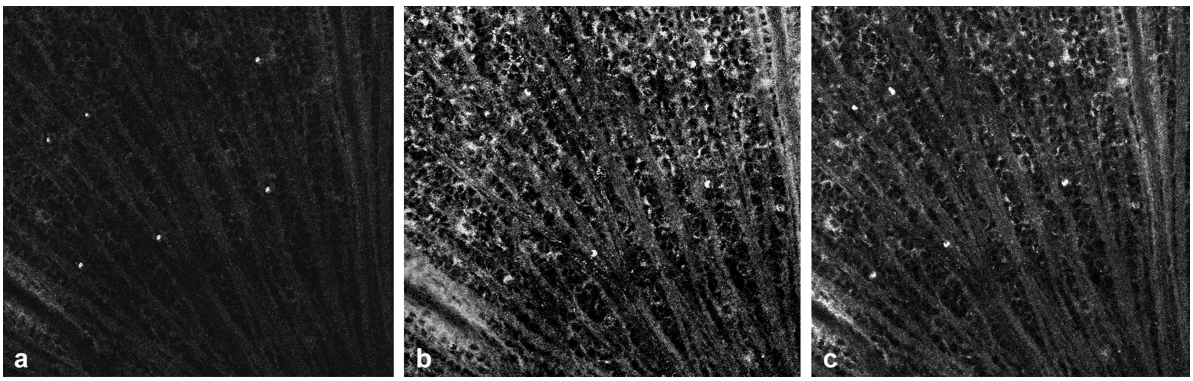

FIGURE 6 **Histologic confirmation that apoptotic cells (a, labeled with Annexin V) were localized to RGC (b, retrogradely labeled with DiI) as shown in the combined micrograph (c) in the SSP model in a mouse.**

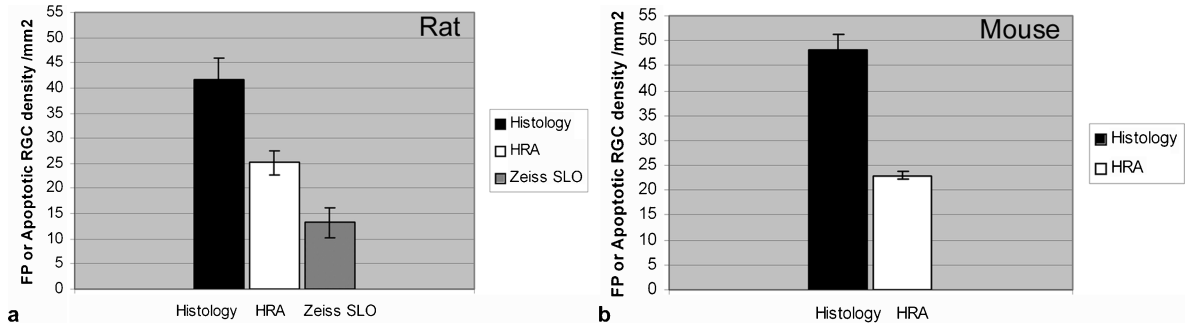

FIGURE 7 **Comparisons between the average apoptotic FP density detected by *in vivo* imaging and average apoptotic RGC density detected by confocal histology. (a) In the rat, confocal histology detects 42 cells/mm^2 compared with HRAII (25 cells/mm^2; 60% of histology) and Zeiss cSLO (13 cells/mm^2; 32% of histology). (b) In the mouse, the HRAII shows 54% (25 apoptotic cells/mm^2) of the confocal histology (48 apoptotic cells/mm^2).**

maximum detection of both machines is at a diameter of 5–10 μm. The greater the diameter, the smaller the detection rate. In comparison with the HRAII, the Zeiss cSLO only detects around 35% of the FPs at 5- to 10-μm point size diameter. However, there is less discrepancy between the two machines at larger diameters. Comparisons of the FP counts in relation to their location in the retina (Fig. 5b, c) show that the HRAII detects most FPs within the superior, temporal, and superior temporal areas. The Zeiss cSLO detects most FPs within the central, superior temporal, and temporal areas, but on average detects 60% less fluorescent signal compared with the HRAII.

Identification of RGCs

Histological analysis was performed in a whole flat-mounted mouse retina 7 days after retrograde labeling and 2 hrs after intraocular SSP treatment for the identification of RGCs. Figure 6 shows double labeling of apoptosing RGCs (Fig. 6a Annexin V) and retrogradely labeled RGCs (Fig. 6b Dil). The overlay (Fig. 6c) confirms that apoptotic cells were localized to the RGC layer.

Comparison of *in vivo* Imaging with Confocal Histology

Comparisons between the average FP densities from the HRAII and the Zeiss cSLO and apoptosing RGC densities from confocal histology were performed in the rat. The HRAII, with 25 FP/mm^2, detects 60% of the confocal histology fluorescence signal (42 cells/mm^2). However, the Zeiss cSLO, with 13 FP/mm^2, only represents 32% of the confocal histology (Fig. 7a). In the mouse model, comparisons were only possible between the HRAII and confocal histology due to the above-mentioned low-quality images obtained with the Zeiss cSLO in the mouse, but showed a similar ratio of FPs to apoptotic cell densities between the HRAII and confocal histology (Fig. 7b). Our results validated that FPs in the *in vivo* images were apoptotic RGCs, confirmed by histology.

DISCUSSION

Our results clearly show that it is possible to visualize apoptosing RGCs in the mouse eye *in vivo*, using our novel technique of imaging.[1,38] We obtained good quality mouse retinal images however only with the HRAII as opposed to the Zeiss cSLO, which we had previously used with our novel technique.[1,38] This has great implications for studying retinal disease models. As far as we are aware, there is no data on visualized mouse RGC undergoing apoptosis *in vivo*. Although conventional fluorescence microscopy has been used to monitor retrograde labeled RGCs over time *in vivo*,[40] only histological studies of RGC apoptosis in mouse models have been described previously.[41,42]

The mouse has developed into an extremely important mammalian model system for genetic and basic cell biology research. Genetic models provide a much more accurate model of chronic disease[43–47] which is difficult to reproduce surgically or chemically. An objective assessment of these models also provides a tool to optimally investigate and monitor potential treatments of the diseases on which these models are based. Specifically, we believe that our technique of imaging RGC apoptosis in the mouse can be utilized in the assessment of potential

neuroprotective strategies in chronic neurodegenerative disorders.[1,30]

Another advantage of using cSLO *in vivo* imaging is it provides a quick estimate of the degree of apoptosis throughout the retina. Historically, histological studies of RGC apoptosis have relied on sample areas of retinal cell counts, which is not an accurate representation of retinal changes, as recently shown by Danias.[47] Histological data in this study were acquired from a relatively large retinal area (40% of whole retina in rat and mouse) and not by relying on sample areas. The total retinal area included in the *in vivo* FP counts in this study covered 15.8 mm^2, which is approximately 40% less than the area of retina we have analyzed histologically in our previous reported studies.[1,35] The total retinal area captured by confocal histology (26.65 mm^2) and implicated for the calculations represents 40% of the whole retina (73.56 mm^2) in rat. In the mouse, the area used for calculations was 21.45 mm^2, again, representing 40% of the whole mouse retina (55.04 mm^2). In this study, we have shown that the HRAII gave around 50–60% counts of what was seen histologically. We are currently refining our technique to get 1:1 correspondence of *in vivo* with histology, and we hope to report on this shortly. The findings here we believe may be attributed to limitations of the *in vivo* imaging instrumentation. The HRAII is designed for the human eye and therefore not optimally aligned for the use of rodent eyes at present, but we have shown with this study that it is possible to use the HRAII for the application of our novel technique of imaging RGC apoptosis in the rat and mouse eye.

Our results show that despite using as similar a setup as possible of both ophthalmoscopes, the HRAII produced higher-quality images with enhanced resolution and contrast. This is similar to Bellmann's recently reported study where they compared three different SLOs including the HRA and the Zeiss cSLO.[28]

The laser output of the Zeiss cSLO was in fact higher with 320 μW than the laser output of the HRAII with 275 μW. Similar observations about the laser power were made by Bellmann et al.[28] Again, despite different laser power outputs, they showed that higher grayscale values were apparent on the HRAII, with reduced background noise measurements compared with the Zeiss.[28] They attributed the differences to different instrument optical pathways and detector sensitivity. Both Zeiss and HRAII instruments use a nonmodified blue argon laser with a wavelength of 488 nm for excitation, with similar barrier filters (500-nm cutoff for the HRAII and 521-nm for the Zeiss cSLO).[1,28]

Although previously the type of photodetector was believed to be an important factor in determining image quality, this is no longer believed to be the case.[28] The HRAII detects 1.9 times more fluorescent signal in rats compared with the Zeiss cSLO suggesting that the sensitivity of the HRAII is greater and therefore more effective. The size distribution of fluorescent points corresponds with histological studies, which suggest the retinal ganglion cell sizes vary between 10 and 23 μm in the rat[49–50] and in mice between 5 and 15 μm.[47,51]

The predominance of fluorescence in the superior area in the rat may be explained by the position of the injection sites and the distribution of the SSP and Annexin V on the retina. This effect may be more important in the rat for reasons related to biodistribution in the eye. Hence, we have calculated that the injection-to-vitreous volume ratio is lower in the rat compared with the mouse (0.07% and 0.12%, respectively). But this may not be the only consideration, as other factors determining intravitreal dosing include compound vitreous velocity, diffusivity, and vitreous anteroposterior length.[52] As the mouse vitreous length is at least 8 times smaller than the rat,[36] intravitreal drugs take a much shorter time to diffuse out of the vitreous. This may explain the more even distribution of the SSP and Annexin V injections in the mouse retina.

Over and above the increased sensitivity of the HRAII, we also believe it has several other advantages over the Zeiss cSLO: firstly, its improved maneuverability enables a larger area (17% more) of the retinal images to be captured compared with the Zeiss cSLO; secondly, its preset calibration permits accurate confocal depth analysis[15,21,53]; and finally, the fact that unlike the Zeiss cSLO prototype, it is commercially available.

However, there are advantages of the Zeiss cSLO, which because of its prototype status makes it suitable for adaptation for custom-build studies. In fact, the Zeiss cSLO was the first machine used to record retinal autofluorescence. Lois and colleagues, by adjusting the imaging area recorded (10 $\times$ 750 pixels), showed that the Zeiss cSLO can be used to construct a fundus autofluorescence topographical map of the posterior pole.[27] We feel that the usability would be even further enhanced by changing the type of stereotaxic frame and the animal holding platform to enable an increased accessibility of the laser head towards the animal eye.

To our knowledge, this study shows for the first time visualized apoptosing retinal ganglion cells in an *in vivo* mouse model. Of particular interest is the improved image quality that we achieved with the HRAII.

Accurate visualization is an important requirement in experimental retinal ganglion cell disease, and there is a necessity for objective data collection when assessing new strategies and therapies. The superior resolution properties of the HRAII compared with the Zeiss cSLO appear advantageous in assessing fluorescent-labeled apoptosing retinal ganglion cells in the mouse with our previously described technique.[1] We think that the technical properties of the HRAII, its improved maneuverability, and the fact that it is already commercially available make the HRAII a potential tool for the early detection and diagnosis of glaucomatous disease in patients.

ACKNOWLEDGMENTS

This work was partially presented at the Glaucoma Society (UK & Eire), Nottingham, December 2005, and was supported by the Wellcome Trust and by Heidelberg Engineering.

REFERENCES

[1] Cordeiro MF, Guo L, Luong V, et al. Real time imaging of single nerve cell apoptosis in retinal neurodegeneration. *Proc Natl Acad Sci U S A*. 2004;101(36):13352–13356.

[2] Vila M, Przedborski S. Targeting programmed cell death in neurodegenerative diseases. *Nat Rev Neurosci*. 2003;4(5):365–375.

[3] Raina AK, Hochman A, Ickes H, et al. Apoptotic promoters and inhibitors in Alzheimer's disease: who wins out? *Prog Neuropsychopharmacol Biol Psychiatry*. 2003;27(2):251–254.

[4] Friedlander RM. Apoptosis and caspases in neurodegenerative diseases. *N Engl J Med*. 2003;348(14):1365–1375.

[5] Quigley HA, Nickells RW, Kerrigan LA, et al. Retinal ganglion cell death in experimental glaucoma and after axotomy occurs by apoptosis. *Invest Ophthalmol Vis Sci*. 1995;36(5):774–786.

[6] Garcia-Valenzuela E, Shareef S, Walsh J, Sharma SC. Programmed cell death of retinal ganglion cells during experimental glaucoma. *Exp Eye Res*. 1995;61(1):33–44.

[7] Vermes I, Haanen C, Steffens-Nakken H, Reutelingsperger C. A novel assay for apoptosis. Flow cytometric detection of phosphatidylserine expression on early apoptotic cells using fluorescein labelled Annexin V. *J Immunol Methods*. 1995;184(1):39–51.

[8] Dunn PM. Wilhelm Conrad Roentgen (1845–1923), the discovery of x rays and perinatal diagnosis. *Arch Dis Child Fetal Neonatal Ed*. 2001;84(2):F138–F139.

[9] mpany CM, McNeil BJ. Advances in biomedical imaging. *JAMA*. 2001;285(5):562–567.

[10] Agapova OA, Kaufman PL, Lucarelli MJ, et al. Differential expression of matrix metalloproteinases in monkey eyes with experimental glaucoma or optic nerve transection. *Brain Res*. 2003;967(1–2):132–143.

[11] Link TM, Majumdar S, Peterfy C, et al. High resolution MRI of small joints: impact of spatial resolution on diagnostic performance and SNR. *Magn Reson Imaging*. 1998;16(2):147–155.

[12] Dumont EA, Reutelingsperger CP, Smits JF, et al. Real-time imaging of apoptotic cell-membrane changes at the single-cell level in the beating murine heart. *Nat Med*. 2001;7(12):1352–1355.

[13] Webb RH, Hughes GW, Delori FC. Confocal scanning laser ophthalmoscope. *Applied Optics*. 1987;26(8):1492–1499.

[14] Sharp PF, Manivannan A, Xu H, Forrester JV. The scanning laser ophthalmoscope–a review of its role in bioscience and medicine. *Phys Med Biol*. 2004;49(7):1085–1096.

[15] Medeiros FA, Zangwill LM, Bowd C, Weinreb RN. Comparison of the GDx VCC scanning laser polarimeter, HRT II confocal scanning laser ophthalmoscope, and stratus OCT optical coherence tomograph for the detection of glaucoma. *Arch Ophthalmol*. 2004;122(6):827–8s37.

[16] Burgoyne CF. Image analysis of optic nerve disease. *Eye*. 2004;18(11):1207–1213.

[17] Dong J, Chihara E. Slope analysis of the optic disc in eyes with ocular hypertension and early normal tension glaucoma by confocal scanning laser ophthalmoscope. *Br J Ophthalmol*. 2001;85(1):56–62.

[18] Yucel YH, Gupta N, Kalichman MW, et al. Relationship of optic disc topography to optic nerve fiber number in glaucoma. *Arch Ophthalmol*. 1998;116(4):493–497.

[19] Weinreb RN, Dreher AW, Bille JF. Quantitative assessment of the optic nerve head with the laser tomographic scanner. *Int Ophthalmol*. 1989;13(1–2):25–29.

[20] Brigatti L, Weitzman M, Caprioli J. Regional test-retest variability of confocal scanning laser tomography. *Am J Ophthalmol*. 1995;120(4):433–440.

[21] Greaney MJ, Hoffman DC, Garway-Heath DF, et al. Comparison of optic nerve imaging methods to distinguish normal eyes from those with glaucoma. *Invest Ophthalmol Vis Sci*. 2002;43(1):140–145.

[22] Holz FG, Bellmann C, Rohrschneider K, et al. Simultaneous confocal scanning laser fluorescein and indocyanine green angiography. *Am J Ophthalmol*. 1998;125(2):227–236.

[23] Bartsch DU, Weinreb RN, Zinser G, Freeman WR. Confocal scanning infrared laser ophthalmoscopy for indocyanine green angiography. *Am J Ophthalmol*. 1995;120(5):642–651.

[24] Bellmann C, Holz FG, Schapp O, et al. [Topography of fundus autofluorescence with a new confocal scanning laser ophthalmoscope]. *Ophthalmologe*. 1997;94(6):385–391.

[25] Dithmar S, Holz FG, Burk RO, et al. [Confocal scanning laser indocyanine green angiography with the Heidelberg retinal angiograph]. *Klin Monatsbl Augenheilkd*. 1995;207(1):11–16.

[26] Delori FC, Fleckner MR, Goger DG, et al. Autofluorescence distribution associated with drusen in age-related macular degeneration. *Invest Ophthalmol Vis Sci*. 2000;41(2):496–504.

[27] Lois N, Halfyard AS, Bird AC, Fitzke FW. Quantitative evaluation of fundus autofluorescence imaged "in vivo" in eyes with retinal disease. *Br J Ophthalmol*. 2000;84(7):741–745.

[28] Bellmann C, Rubin GS, Kabanarou SA, et al. Fundus autofluorescence imaging compared with different confocal scanning laser ophthalmoscopes. *Br J Ophthalmol*. 2003;87(11):1381–1386.

[29] von Ruckmann A, Fitzke FW, Bird AC. In vivo fundus autofluorescence in macular dystrophies. *Arch Ophthalmol*. 1997;115(5):609–615.

[30] Guo L, Salt TE, Maass A, et al. Assessment of neuroprotective effects of glutamate modulation on glaucoma-related retinal ganglion cell apoptosis in vivo. *Invest Ophthalmol Vis Sci*. 2006;47:626–633.

[31] Bedell MA, Jenkins NA, Copeland NG. Mouse models of human disease. Part I: techniques and resources for genetic analysis in mice. *Genes Dev*. 1997;11(1):1–10.

[32] Soucy E, Wang Y, Nirenberg S, et al. A novel signaling pathway from rod photoreceptors to ganglion cells in mammalian retina. *Neuron*. 1998;21(3):481–493.

[33] Tagawa Y, Sawai H, Ueda Y, et al. Immunohistological studies of metabotropic glutamate receptor subtype 6-deficient mice show no abnormality of retinal cell organization and ganglion cell maturation. *J Neurosci*. 1999;19(7):2568–2579.

[34] Malek G, Johnson LV, Mace BE, et al. Apolipoprotein E allele-dependent pathogenesis: a model for age-related retinal degeneration. *Proc Natl Acad Sci USA*. 2005;102(33):11900–11905.
[35] Guo L, Moss SE, Alexander RA, et al. Retinal ganglion cell apoptosis in glaucoma is related to intraocular pressure (IOP) and IOP-induced effects on extracellular matrix. *Invest Ophthalmol Vis Sci*. 2005;46(1):175–182.
[36] Remtulla S, Hallett PE. A schematic eye for the mouse, and comparisons with the rat. *Vision Res*. 1985;25(1):21–31.
[37] Ridder W 3rd, Nusinowitz S, Heckenlively JR. Causes of cataract development in anesthetized mice. *Exp Eye Res*. 2002;75(3):365–370.
[38] Guo L, Tsatourin V, Luong V, et al. En-face optical coherence tomography (OCT): a new method to analyze structural changes of the optic nerve head in rat glaucoma. *Br J Ophthalmol*. 2005;89:1210–1216.
[39] Bland JM, Altman DG. Measuring agreement in method comparison studies. *Stat Methods Med Res.* 1999;8(2):135–160.
[40] Thanos S, Indorf L, Naskar R. In vivo FM: using conventional fluorescence microscopy to monitor retinal neuronal death *in vivo*. *Trends Neurosci*. 2002;25(9):441–444.
[41] Reichstein DA, Ren L, Mittag T, Danias J. Visualization of retinal ganglion cell apoptosis in aging glaucomatous DBA/2J mice. ARVO. Fort Lauderdale, FL, 2005.
[42] Chang B, Smith R, Hawes N, et al. Interacting loci cause severe iris atrophy and glaucoma in DBA/2J mice. *Nat Genet*. 1999;21(4):405–409.
[43] Taniguchi T, Doe N, Matsuyama S, et al. Transgenic mice expressing mutant (N279K) human tau show mutation dependent cognitive deficits without neurofibrillary tangle formation. *FEBS Lett*. 2005;579(25):5704–5712.
[44] Fischer DF, Hol EM, Hobo B, van Leeuwen FW. Alzheimer-associated APP+1 transgenic mice: frameshift beta-amyloid precursor protein is secreted in cerebrospinal fluid without inducing neuropathology. *Neurobiol Aging*. 2005;5:5.
[45] Meissner KK, Kirkham DL, Doering LC. Transplants of neurosphere cell suspensions from aged mice are functional in the mouse model of Parkinson's. *Brain Res*. 2005;1057(1–2):105–112.
[46] Masliah E, Rockenstein E, Adame A, et al. Effects of alpha-synuclein immunization in a mouse model of Parkinson's disease. *Neuron*. 2005;46(6):857–868.
[47] Danias J, Lee KC, Zamora MF, et al. Quantitative analysis of retinal ganglion cell (RGC) loss in aging DBA/2NNia glaucomatous mice: comparison with RGC loss in aging C57/BL6 mice. *Invest Ophthalmol Vis Sci*. 2003;44(12):5151–5162.
[48] Huxlin KR, Goodchild AK. Retinal ganglion cells in the albino rat: revised morphological classification. *J Comp Neurol*. 1997;385(2):309–323.
[49] Perry VH. The ganglion cell layer of the retina of the rat: a Golgi study. *Proc R Soc Lond B Biol Sci*. 1979;204(1156):363–375.
[50] Thanos S. Alterations in the morphology of ganglion cell dendrites in the adult rat retina after optic nerve transection and grafting of peripheral nerve segments. *Cell Tissue Res*. 1988;254(3):599–609.
[51] Osborne NN, Chidlow G, Wood JP, et al. Expectations in the treatment of retinal diseases: neuroprotection. *Curr Eye Res*. 2001;22(5):321–332.
[52] Xu J, Heys JJ, Barocas VH, Randolph TW. Permeability and diffusion in vitreous humor: implications for drug delivery. *Pharm Res*. 2000;17(6):664–669.
[53] Zangwill LM, Bowd C, Berry CC, et al. Discriminating between normal and glaucomatous eyes using the Heidelberg Retina Tomograph, GDx Nerve Fiber Analyzer, and Optical Coherence Tomograph. *Arch Ophthalmol*. 2001;119(7):985–993.